ChemComm

COMMUNICATION

View Article Online
View Journal | View Issue

Cite this: *Chem. Commun.*, 2016, 52, 6934

Received 5th April 2016,
Accepted 29th April 2016

DOI: 10.1039/c6cc02824a

www.rsc.org/chemcomm

Aligning self-assembled gelators by drying under shear†

Emily R. Draper,[a] Oleksandr O. Mykhaylyk[b] and Dave J. Adams*[a]

We show how drying under shear can be used to prepare aligned fibres and worm-like micelles from low molecular weight gelators. Shearing followed by drying leads to the dealignment before the water can be removed; continuous shear whilst drying is required to maintain the alignment. Combining a slow pH change with continuous shear allows alignment of the gelling fibres, which can then be dried.

Preparing aligned domains of self-assembled structures is useful for preparing conductive materials,[1] as well as for applications in cell culturing[2,3] amongst others. Gelation *via* the use of low molecular weight gelators (LMWG) is one method of forming long, anisotropic structures that could be amenable to alignment.[4] A range of techniques can be used to align anisotropic structures, including spin-coating, shear, electrical currents, gravity and magnetic fields.[5,6] Preparing large domains of aligned gels has been achieved by pipetting liquid crystalline solutions of self-assembled peptides into a salt bath, relying on the shear forces to align the structures.[7] However, in general preparing aligned gels is difficult as the trigger for gelation to occur needs to be applied whilst aligning the structures. This can be achieved by gelling in a magnetic field, although this is limiting, as very strong magnetic fields are usually required.[8–10]

We have recently described a number of perylene bisimide (PBI) based gelators (Fig. 1).[11] The self-assembly of PBIs is interesting for generating useful electronic materials,[12,13] in areas including organic solar cells, in field-effect transistors, and as well as photocatalysts.[14–16] PBIs absorb strongly in the visible spectrum, have long fluorescence lifetimes and high quantum yields. PBIs are n-type materials, readily accepting electrons to form the radical anion or dianion.[17] In water, our PBIs form worm-like micelles at high pH (typically >8), and gels when the pH is lowered to around 4 (Fig. 1; see Fig. S3, ESI†).[11]

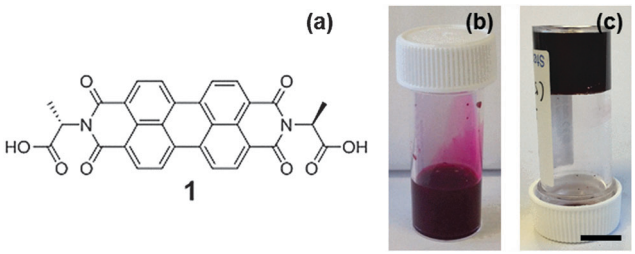

Fig. 1 (a) Structure of PBI **1**; (b) photograph of a solution of **1** in water at pH 9 at 5 mg mL^{-1}; (c) photograph of the corresponding gel at pH 4. The scale bar represents 1 cm.

The gels are the result of an entangled fibrous network being formed at low pH. In both the worm-like micelle and gel fibres, there is significant π-stacking between the PBIs.[11] For many applications where conductive materials are used, alignment of the structures would be ideal; a more aligned sample will show increased conductivity compared to an unaligned sample, as the path the electron has to travel is shorter and there is less chance of recombination of the charges.

In a device, PBIs are often used in the dry state.[16] However, whilst drying either our PBI solutions or gels resulted in photoconductive films,[11] alignment of the structures was difficult. For the gel especially, drying the entangled fibres to give a xerogel film resulted in a randomly aligned network. Whilst aligned PBIs have been reported,[18–20] aligning PBI aggregates can be very difficult using conventional techniques,[21,22] which restricts the use of PBIs.

In an attempt at forming aligned films from our PBIs, we investigated common methods including spin coating, gravitational alignment and doctor blading. All these methods rely on the solvent in which the material is dissolved (here, water) evaporating sufficiently quickly such that the alignment created is maintained. None of these methods were successful (example data for spin-coated samples are shown in Fig. S4, ESI†). A similar lack of success has been reported for similar PBI aggregates previously.[21,22] A more effective method of alignment is therefore needed. Hence, we investigated shear alignment.[23–25]

[a] *Department of Chemistry, University of Liverpool, Crown Street, Liverpool, L69 7ZD, UK. E-mail: d.j.adams@liverpool.ac.uk*
[b] *Department of Chemistry, University of Sheffield, Sheffield, S3 7HF, UK*
† Electronic supplementary information (ESI) available. See DOI: 10.1039/c6cc02824a

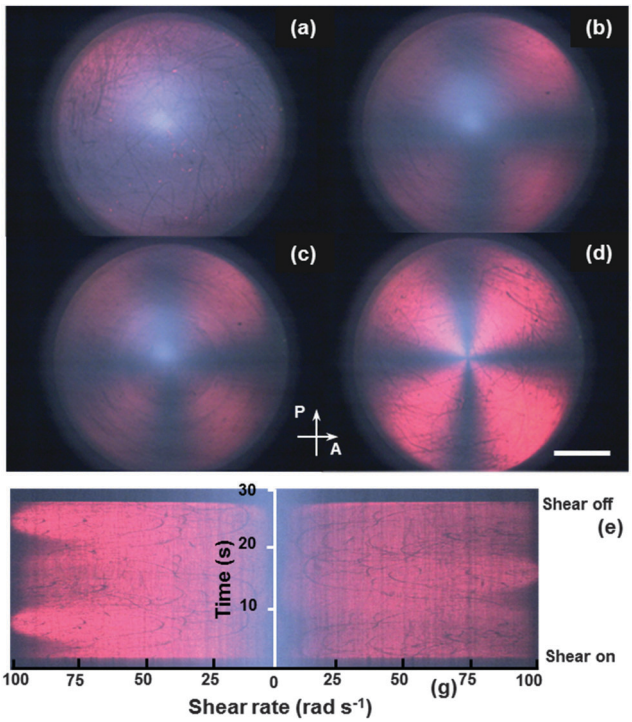

Fig. 2 Polarised light images (PLIs) of solutions of **1** in water at pH 9 under shear using a 25 mm parallel disks rotating at angular speed of 1.6 rad s^{-1} with a 0.2 mm gap distance (maximum shear rate 100 s^{-1}) at 25 °C (a) 5 mg mL^{-1}, (b) 10 mg mL^{-1}, (c) 30 mg mL^{-1}, and (d) 40 mg mL^{-1}. Scale bar represent 5 mm. The vectors labelled by letters P and A are a polarizer and an analyzer axis, respectively; (g) A time sliced PLIs of a 10 mg mL^{-1} solution of **1** under a shear pulse for 25 seconds.

As worm-like micelles are present in the solutions of **1** (Fig. S3, ESI†),[11] if sufficient shear rate is applied, then these should align with the direction of shear flow. However, to prepare an aligned film, as noted the alignment needs to be maintained such that drying is possible.

We utilised rheo-optics to visualise the shear alignment (Fig. 2). A mechanical rheometer (Anton Paar Physica MCR 301) combined with shear-induced polarized light imaging (SIPLI) technique[26,27] is used where the bottom static plate of the rheometer is glass, with a camera, linear polarizer and light source attached to image the sample. The solution was placed between the two parallel plates on the rheometer and shear applied by rotating the top plate. When the solution is perfectly aligned, and the optical axis of the studied morphologies is preferably oriented along the flow directions, a Maltese cross indicating birefringence of the sheared sample is visible. The light intensity of the polarized light image (PLI) is proportional to the degree of alignment, as well as to the concentration of sample used. This measurement was performed on solutions of **1** at pH 8 at concentrations of 5, 10, 30, and 40 mg mL^{-1} (Fig. 2).

When a maximum shear rate of 100 s^{-1} was applied to the samples for 30 seconds using a 25 mm parallel plate, alignment occurred in all samples. The solution at 5 mg mL^{-1} (Fig. 2a) showed the least alignment under these conditions, providing the dullest picture, whereas the 40 mg mL^{-1} (Fig. 2d) showed the highest degree of alignment with the brightest, most defined Maltese cross. Alignment can be achieved at different gap distances (Fig. S5, ESI†); here we optimised the thickness to 0.2 mm.

The shear alignment images were further analysed and processed using the image analysis software ImageJ. A slice of each image at a 45° angle to the Maltese cross was taken and then combined to produce one image representing the shear experiment[20,21] (Fig. 2e); the horizontal axis is the shear rate and the vertical axis, coinciding with the axis of rotation, is time. It can be seen that the central part of the sliced images, associated with small shear rates, is relatively dark and non-birefringent suggesting no sample alignment occurs at these shear conditions and a shear rate of 10 s^{-1} or more is needed for alignment, (*i.e.* where the image is consistently bright). These data also show that alignment happens very quickly when shear is applied, but alignment is lost in a fraction of a second after the shear is stopped. This quick recovery explains why alignment methods such as doctor blading, and spin coating were unsuccessful, as the sample recovers faster than the solvent can evaporate. This also highlights differences between our systems and others, where alignment was not lost after cessation of the shear[28] and the sample could be simply allowed to dry. We believe that this is due to the fact that previous systems contained liquid crystalline materials, which presumably only lose their alignment very slowly. However, most LMWG do not form liquid crystalline phases at the concentrations typically used. We also highlight that the on/off rates of the self-assembled structures may be different.

To overcome the problem of the solution recovering quickly after shear, we hypothesised that the solution could be dried under a constant shear. This was achieved using a cone and plate geometry on a rheometer. A solution of **1** at a concentration of 10 mg mL^{-1} was used, as this was the lowest concentration that gave a clear Maltese cross (Fig. 2b). To prepare the aligned dried solution, a removable piece of glass was attached to the bottom plate of the rheometer. The solution was placed on the glass and the cone geometry lowered onto the solution. In order to reduce the chance of damaging the film as the film dried a minimum shear rate of 10 s^{-1} (defined from SIPLI measurements, Fig. 2b) was applied. The shear experiment was performed overnight whilst all the water evaporated from the sample. After the solution was dry, the glass was removed from the rheometer and the sample could be viewed on the microscope where aligned rings of material can be seen (Fig. 3a). Under cross-polarised light (Fig. 3c and d), these aligned rings are clear and brightly coloured showing alignment of the material. This method of shear alignment was highly reproducible. Imaging the structures using SEM, it is clear that the rings are formed from aligned micelles (Fig. S6, ESI†). The alignment is also consistent throughout the entire depth of the sample (Fig. S7, ESI†).

Photoresponse measurements were then performed on these samples. The photoconductivity was measured both along and perpendicular to the alignment by placing silver electrodes either side of the aligned structures (as determined by microscopy) and above and below the aligned structure (Fig. S1, ESI†). The decrease in resistance was measured when the samples

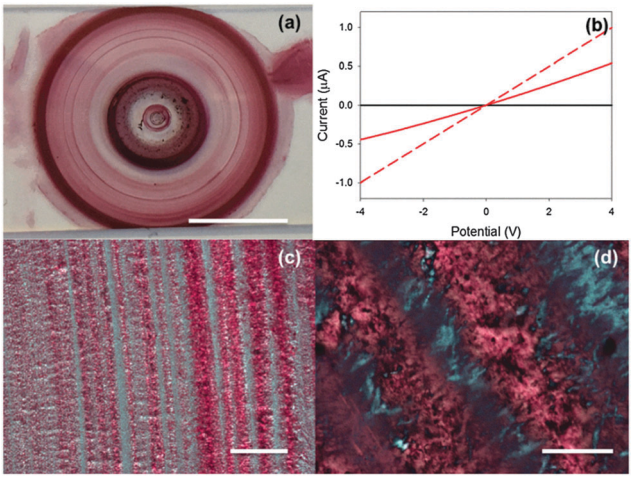

Fig. 3 (a) Photograph of dried solution of **1** after shearing for 16 hours. Scale bar represents 1 cm. (b) Photoresponse of the shear aligned dried solution of **1**. Black data is in the dark and red data is under 365 nm light. Solid red data is against alignment and red dashed data is with alignment. (c and d) Optical microscope images of (a) viewed under cross-polarised light. The scale bars in (c) and (d) correspond to 0.2 mm and 50 μm, respectively.

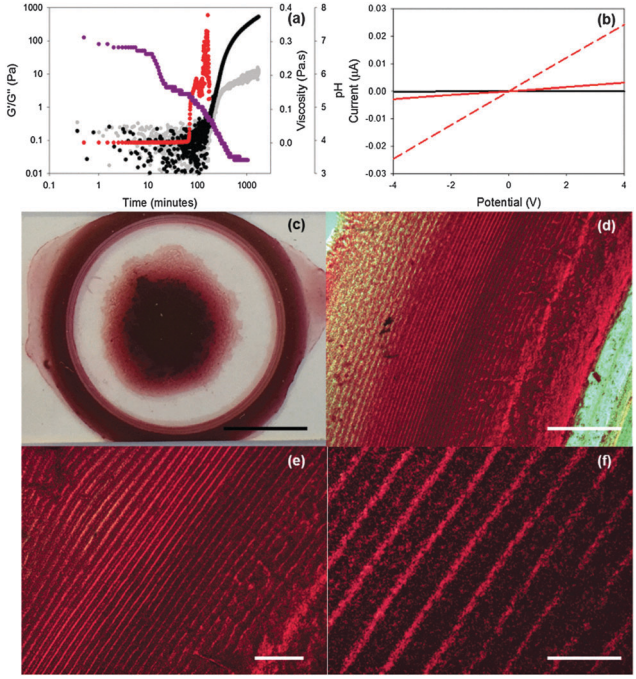

Fig. 4 (a) Development of G' (black data) and G'' (grey data) over time during the gelation of **1** at a strain of 0.5% and a frequency of 10 rad s^{-1}, compared to change in viscosity (red data) and change in pH (purple data) over time; (b) photoresponse of xerogel-**1** at a concentration of 10 mg mL^{-1} (left) gelled under shear and (right) without shear. Black data is in the dark and red data is under 365 nm light. Solid red data is against alignment and red dashed data is with alignment. (c) Photograph of the edge of the xerogel **1** after shearing for 2 hours. Scale bar represents 1 cm. (d–f) Optical microscope images of (c) under cross-polarised light. The scale bars in (b), (c) and (d) correspond to 0.5 mm, 0.2 mm and 50 μm, respectively.

were irradiated using a 365 nm LED (at higher wavelengths, the samples are not appreciably photoconductive as we discussed previously[11]). By measuring the amount of material between the electrodes, differences in the absolute volume of **1** used was found not to affect the conductivity (Fig. S8, ESI†). Similarly, differences in sample thickness were found not to correlate with the conductivity (Fig. S9, ESI†). Hence, differences in the conductivity with and against the alignment are due to how aligned the self-assembled aggregates are.

To quantify this directional dependence on photoresponse, the value at −4 V taken for the measurement against alignment was divided by the value at −4 V for the measurement with alignment. We define this value as S; the closer to zero S is, the greater the alignment. Fig. 3e shows that the sample has a value of S of around 0.60. This is higher than seen for the coffee-ring aligned samples (S = 0.32; Fig. S10 and S12, ESI†) produced previously.[11] This method however was found to be much more reproducible and always gave aligned structures with similar values of S. We ascribe this to there being fewer variables when drying under shear.

We then moved on to forming gels under shear. As noted above, **1** forms gels at low pH. When lowering the pH of the sample under shear, the sample needs sufficient time under shear to gel but not too long a time that it disrupts the gel structures. The sample does not need to dry under shear as gelation should lock in any aligned structures formed. To lower the pH and induce gelation, we used glucono-δ-lactone (GdL), which hydrolyses slowly to gluconic acid.[29,30] This method of pH change is highly reproducible as we have described in detail previously.[29] After adding GdL to a solution of **1**, the change in viscosity was measured. The viscosity data is useful as it senses a development of structures in solution (Fig. 4a).

The solution shows virtually the same viscosity as water until 65 minutes when the viscosity rapidly increases. During this time, the solution has reached the first pK_a at pH 6.7 of the gelator (Fig. S13, ESI†). As pH drops to the second pK_a at pH 5.4, the viscosity sharply increases as larger structures start to form. At 90 minutes, the storage modulus (G') and loss modulus (G'') start to increase as gelation begins. At this point, there is then a decrease in viscosity as the gelling fibres start to align under the shear (the viscosity overshoot). The viscosity then increases again as the gel is developing further until 130 minutes.

After 130 minutes, the viscosity data are not reliable due to gelation occurring. According to the gelation time sweep data, G' is an order of magnitude larger than G'' at around 300 minutes (pH 3.6), showing gelation has occurred. To summarize the data, larger structures form after 60 minutes and gelation occurs after 300 minutes. Alignment of these structures can be identified in the viscosity data at 130 minutes. Hence, shear alignment experiments need to be performed for between 130 and 300 minutes. A shear was therefore applied to the samples for between 120 and 180 minutes using a 25 mm cone geometry at a constant shear rate of 10 s^{-1}. When samples were sheared for less time than this, gelation had not occurred and the sample was still liquid (Fig. S14a, ESI†). Applying shear for longer than 210 minutes resulted in the gel sample being damaged (Fig. S14b, ESI†). Gels sheared for 150 minutes showed the same ringed pattern as seen with the dried solutions (Fig. 3b) but also had a denser area of gel

in the middle. These samples were allowed to dry in air to give shear-aligned xerogels. When viewed under cross-polarised light, they showed aligned structures (Fig. 4c and d). This is very different to the samples formed without shear (Fig. S10 and S12, ESI†). Again, SEM showed that the underlying structures are highly aligned (Fig. S15, ESI†). When photoresponse measurements were performed on shear-aligned xerogels, they showed a significant directional dependence (Fig. 4b). This is different to when gelation occurs in the absence of shear (Fig. S12e, ESI†). Shear aligned xerogels have a directional dependence, S, of between 0.06 and 0.12, compared to xerogels not gelled under shear (S = 0.95, Fig. S12e, ESI†). This method gave very reproducible samples, which maintain their conductivity and alignment with time. Samples measured 6 months later showing very similar conductivities and directional dependence (Fig. S16, ESI†).

The shear aligned xerogels also show a better and more reproducible directional dependence than the shear aligned and drop-cast dried solutions. We hypothesise that this is due to the fibres being longer than in the worm-like micelles in the solution state and so are more able to align. However, the absolute conductivities are lower for the gels compared to the solutions; we ascribe these differences in the photoresponse to different fibre morphologies and/or how densely packed the fibres are. To answer both of these questions however, more investigation is needed.

Hence, we have shown that we can align both the worm-like micelles and the gelled fibrous structures of a PBI using shear forces. Rheo-optic measurements show that the aligned morphology relaxes in a fraction of seconds once the shear forces are removed. This explains our lack of success using methods such as spin coating to align the samples, and probably also explains the difficulties reported elsewhere in preparing aligned PBI films. Hence, to prepare aligned, dried films, the drying process must be performed under shear which can easily be achieved using a cone and plate geometry. This differs from previous examples where drying post shear was possible, presumably due to the presence of a liquid crystalline phase that did not lose alignment quickly.[28] We have shown that the slow pH change that can be achieved with GdL allows us to also prepare well aligned gelled fibres, which is extremely difficult to do by other methods. To the best of our knowledge, this is the first examples where alignment of the same molecular PBI at different pH and assembled state has been achieved. The control over the degree of alignment results in photoconductive films with significantly improved properties as compared to air-dried films. Hence, these methods of alignment give well-defined structures that could be used in electronic devices. These approaches should be amenable to many other gelling systems and we expect that this method could be used to prepare aligned films using similar gelators, which could be used for many applications, for example cell growth.[3]

ED thanks the EPSRC for a DTA studentship. DA thanks the EPSRC for a fellowship (EP/L021978/1). OM thanks Anton Paar Ltd (Graz, Austria) for the donated rheometer.

Notes and references

1 S. Takami, S. Furumi, Y. Shirai, Y. Sakka and Y. Wakayama, *J. Mater. Chem.*, 2012, **22**, 8629–8633.
2 D. Ceballos, X. Navarro, N. Dubey, G. Wendelschafer-Crabb, W. R. Kennedy and R. T. Tranquillo, *Exp. Neurol.*, 1999, **158**, 290–300.
3 S. Oh, C. Daraio, L.-H. Chen, T. R. Pisanic, R. R. Fiñones and S. Jin, *J. Biomed. Mater. Res., Part A*, 2006, **78A**, 97–103.
4 S. S. Babu, V. K. Praveen and A. Ajayaghosh, *Chem. Rev.*, 2014, **114**, 1973–2129.
5 L. Jiang, H. Dong and W. Hu, *Soft Matter*, 2011, **7**, 1615–1630.
6 L. Hu, R. Zhang and Q. Chen, *Nanoscale*, 2014, **6**, 14064–14105.
7 S. Zhang, M. A. Greenfield, A. Mata, L. C. Palmer, R. Bitton, J. R. Mantei, C. Aparicio, M. O. de la Cruz and S. I. Stupp, *Nat. Mater.*, 2010, **9**, 594–601.
8 D. W. P. M. Löwik, I. O. Shklyarevskiy, L. Ruizendaal, P. C. M. Christianen, J. C. Maan and J. C. M. van Hest, *Adv. Mater.*, 2007, **19**, 1191–1195.
9 M. Wallace, A. Z. Cardoso, W. J. Frith, J. A. Iggo and D. J. Adams, *Chem. – Eur. J.*, 2014, **20**, 16484–16487.
10 Y. Kitahama, Y. Kimura, K. Takazawa and G. Kido, *Bull. Chem. Soc. Jpn.*, 2005, **78**, 727–730.
11 E. R. Draper, J. J. Walsh, T. O. McDonald, M. A. Zwijnenburg, P. J. Cameron, A. J. Cowan and D. J. Adams, *J. Mater. Chem. C*, 2014, **2**, 5570–5575.
12 F. Würthner, C. R. Saha-Möller, B. Fimmel, S. Ogi, P. Leowanawat and D. Schmidt, *Chem. Rev.*, 2016, **116**, 962–1052.
13 S. Chen, P. Slattum, C. Wang and L. Zang, *Chem. Rev.*, 2015, **115**, 11967–11998.
14 F. Wurthner, *Chem. Commun.*, 2004, 1564–1579.
15 A. W. Hains, Z. Liang, M. A. Woodhouse and B. A. Gregg, *Chem. Rev.*, 2010, **110**, 6689–6735.
16 C. Huang, S. Barlow and S. R. Marder, *J. Org. Chem.*, 2011, **76**, 2386–2407.
17 M. Supur and S. Fukuzumi, *ECS J. Solid State Sci. Technol.*, 2013, **2**, M3051–M3062.
18 R. Marty, R. Szilluweit, A. Sánchez-Ferrer, S. Bolisetty, J. Adamcik, R. Mezzenga, E.-C. Spitzner, M. Feifer, S. N. Steinmann, C. Corminboeuf and H. Frauenrath, *ACS Nano*, 2013, **7**, 8498–8508.
19 A. M. Kendhale, A. P. H. J. Schenning and M. G. Debije, *J. Mater. Chem. A*, 2013, **1**, 229–232.
20 D. Dasgupta, A. M. Kendhale, M. G. Debije, J. ter Schiphorst, I. K. Shishmanova, G. Portale and A. P. H. J. Schenning, *ChemistryOpen*, 2014, **3**, 138–141.
21 Y. Zakrevskyy, C. F. J. Faul, Y. Guan and J. Stumpe, *Adv. Funct. Mater.*, 2004, **14**, 835–841.
22 A. Laiho, B. M. Smarsly, C. F. J. Faul and O. Ikkala, *Adv. Funct. Mater.*, 2008, **18**, 1890–1897.
23 P. LeDuc, C. Haber, G. Bao and D. Wirtz, *Nature*, 1999, **399**, 564–566.
24 G. G. Barclay, S. G. McNamee, C. K. Ober, K. I. Papathomas and D. W. Wang, *J. Polym. Sci., Part A: Polym. Chem.*, 1992, **30**, 1845–1853.
25 D. J. Alt, S. D. Hudson, R. O. Garay and K. Fujishiro, *Macromolecules*, 1995, **28**, 1575–1579.
26 O. O. Mykhaylyk, *Soft Matter*, 2010, **6**, 4430–4440.
27 O. O. Mykhaylyk, A. J. Parnell, A. Pryke and J. P. A. Fairclough, *Macromolecules*, 2012, **45**, 5260–5272.
28 I. K. Iverson, S. M. Casey, W. Seo, S.-W. Tam-Chang and B. A. Pindzola, *Langmuir*, 2002, **18**, 3510–3516.
29 D. J. Adams, M. F. Butler, W. J. Frith, M. Kirkland, L. Mullen and P. Sanderson, *Soft Matter*, 2009, **5**, 1856–1862.
30 Y. Pocker and E. Green, *J. Am. Chem. Soc.*, 1973, **95**, 113–119.